eNeuro

*Research Article: New Research | Cognition and Behavior*

# Exploring the role of the nucleus accumbens in adaptive behavior using concurrent intracranial and extracranial electrophysiological recordings in humans

https://doi.org/10.1523/ENEURO.0105-20.2020

**Cite as:** eNeuro 2020; 10.1523/ENEURO.0105-20.2020

Received: 18 March 2020
Revised: 8 September 2020
Accepted: 10 September 2020

# Exploring the role of the nucleus accumbens in adaptive behavior using concurrent intracranial and extracranial electrophysiological recordings in humans

**Abbreviated title**

Role of the nucleus accumbens in adaptive behavior

**Nadine Eijsker*[1,2], Guido van Wingen[1,2], Ruud Smolders[1,2], Dirk J.A. Smit[1,2], and Damiaan Denys[1,2]**

[1] Amsterdam UMC, University of Amsterdam, Department of Psychiatry, Amsterdam Neuroscience, Amsterdam, the Netherlands

[2] Amsterdam Brain and Cognition, University of Amsterdam, Amsterdam, the Netherlands

***Corresponding author**

Nadine Eijsker, Meibergdreef 9, 1105 AZ, Amsterdam, the Netherlands

+31 20 8913668

nadine.eijsker@gmail.com

**Media and word count**

This manuscript includes 3 figures and 4 tables. Abstract = 151, introduction = 548, discussion = 1700.

**Acknowledgements**

The authors thank all patients for their participation.

**Competing Interests**

The authors declare no competing financial interests.

**Funding sources**

The authors received no financial support for the research, authorship, and/or publication of this article.

## Abstract

Recent human electrophysiological evidence implicated theta-band communication between the Nucleus Accumbens (NAc) and frontal and parietal cortex in cognitive flexibility. Since the NAc is connected with the motor system, we tested whether phase and amplitude-based NAc-cortical connectivity and power modulation likewise underlie flexibility in motor action control. We combined concurrently recorded intracranial and extracranial electroencephalograms from seven psychiatric patients implanted with deep brain stimulation electrodes who performed a stop signal task. Inhibition success – as opposed to failure – was associated with greater pre-stimulus information flow from right NAc to medial frontal cortex through phase coupling of theta oscillations. Inhibition failure evoked theta power increases in the left NAc and medial frontal cortex, whereas parieto-occipital cortex showed an alpha power decrease. We conclude that NAc-to-frontal theta connectivity, possibly facilitating processing of task-relevant information, and alpha and theta power modulations, possibly reflecting post-error engagement of cognitive control, contribute to adaptive behavior pertaining motor control.


## Significance statement

Combining unique intracranial recordings from human nucleus accumbens and concurrently recorded electroencephalographic data, we complement previous research on the involvement of nucleus accumbens-cortical theta-band communication in adaptive behavior by showing that pre-stimulus theta phase synchronization likely drives this process.

## Introduction

The Nucleus Accumbens (NAc) has a well-established role in reward processing and reinforcement learning (Cohen et al., 2008; Lega et al., 2011; Cohen et al., 2012; Patel et al., 2012). Yet, in recent years, it has additionally been implicated in cognitive flexibility (Floresco et al., 2006; van Schouwenburg et al., 2010; Yawata et al., 2012; Horschig et al., 2015). Specifically, interplay between the NAc and prefrontal cortex seems important for flexibility. The prefrontal cortex is thought to exert cognitive control by strategy development and active maintenance of goal-relevant representations (Miller and Cohen, 2001) and projects directly to the NAc, whereas the NAc seems to actively gate such task-relevant information (van Schouwenburg et al., 2010; Horschig et al., 2015) and indirectly projects back to frontal and parietal cortex via the globus pallidus, subthalamic nucleus and the medial dorsal nucleus of the thalamus (Alexander et al., 1986; Haber et al., 1995; Haber and Knutson, 2010). This idea was previously corroborated and extended using human intracranial electrophysiological data to show that the NAc increased theta-band communication to the neocortex – primarily frontal cortex and additionally parieto-occipital cortex- upon processing of visual stimuli in a task requiring an attentional switch (Horschig et al., 2015). Moreover, these regions communicated with the NAc in the alpha-band during anticipation of visual processing.

Considering its connections, the NAc is seen as a functional link between the limbic and motor systems (Mogenson et al., 1980), yet the previously employed tasks only probed cognitive flexibility. Electrophysiological evidence for the involvement of the subthalamic nucleus – part of the motor system via which the NAc projects to the cortex - has already been found on a stop signal task (SST; Ray et al., 2012), a frequently adopted paradigm to study the ability to inhibit an ongoing motor response in the face of changing demands (response inhibition). Based on the NAc's involvement in cognitive flexibility and its connections to the motor system, we tested whether the NAc is likewise involved in flexibility that pertains motor action directly. We likewise adopted the SST, which requires balancing speed (rapid response to a go-signal initiating action) and accuracy (successful inhibition of an ongoing response following a stop signal). The task is theoretically grounded in the

74 horse-race model (Logan and Cowan, 1984), which posits that response inhibition depends on the
75 relative finishing times of independent and competing go and stop processes. However, it may not be
76 that simple; studies have found stimulus detection and action selection and execution to be
77 influenced by both proactive and reactive control processes, with responses often being slowed in
78 order to balance accuracy and speed (Bissett and Logan, 2011).

79 NAc-targeted deep brain stimulation (DBS) in compulsive and depressed patients offers the
80 unique opportunity of recording intracranial EEG (iEEG) from the human NAc and surrounding area.
81 Since bidirectional cortico-striatal communication seems essential for optimization of flexible
82 behavior, we combined intracranial and surface EEG recordings from psychiatric patients to
83 investigate amplitude and phase-based cortico-striatal communication and power modulation during
84 SST performance. If the role of the NAc in behavioral flexibility is similar to that in cognitive flexibility,
85 we expect 1) alpha-band connectivity, specifically information flow from the cortex towards the NAc,
86 during anticipation of stimulus presentation, followed by 2) theta-band connectivity, specifically
87 information flow from the NAc towards the cortex, during stimulus processing.

88

89 ## Methods

90 **Participants**

91 Ten treatment-refractory psychiatric patients were recruited from the Academic Medical Center
92 outpatient clinic. Two participants were excluded based on performance; one successfully inhibited
93 on over 90% of stop trials, whereas the other completely lacked successful stop trials, resulting in too
94 few trials in the remaining condition to analyze. Another participant displayed extreme amounts of
95 beta-band oscillations due to brain tumor removal. Of the remaining seven participants (aged 22-63
96 years; five females and two males), four were diagnosed with obsessive-compulsive disorder (one
97 with comorbid obsessive-compulsive personality disorder), two patients with major depressive
98 disorder, and one patient with cocaine and opiate addiction (table 1). All participants were right-
99 handed and took their standard medication, with the exception of selective serotonin reuptake

inhibitors. Medications included Euthyrox 50 mcg/day, Omeprazole 40 mg/day, Simvastatin 20 mg, Triazolam 100 mg/day, Suboxone 4mg/day, Flucloxacilline 1000mg/four daily, Nifedipine 40 mg/day, Selokeen 50 mg/day, Omeprazole 20 mg/day, Melatonin 5 mg/day, Promethazine 25 mg/day, Lorazepam 2,5 mg/day, Seroquel 300 mg/day, Parnate 30 mg/two daily, Domperidon 10 mg/day, and Movicolon and Paracetamol where necessary.

The local Medical Ethical Committee of the Academic Medical Center approved the experiment and all participants provided written informed consent prior to the experiment.

**Stop signal task**

*Stimulus presentation*

Stimuli were presented using Presentation (Version 14.5; Neurobehavioral Systems, Inc.) on a 15.4 inch-laptop (HP 6730b) screen, placed approximately 60 cm from the participants, at a resolution of 1024 by 768 pixels and with a refresh rate of 60 Hz.

*Task properties*

The SST consists of two types of trials. In go trials, a green arrow (go stimulus) pointing either to the left or right signals participants to press the corresponding - left or right – shift button on a keyboard as fast as possible using their left and right index fingers, respectively. In stop trials, the arrow changes color from green to red (stop stimulus) after a variable delay; the stop signal delay (SSD). This signals participants to cancel their motor response to the go stimulus. Participants were instructed to respond to go signals as fast as possible, while simultaneously minimizing inhibition failures, and that these two criteria were equally important.

Our task consisted of three blocks of 100 trials each, of which 70% go trials and 30% stop trials. The inter-trial-interval, during which a fixation cross was presented, varied randomly between 1750, 1875, 2000, 2125, and 2250 ms, with each interval presented equally often. Go stimuli were presented until response or a stop stimulus appeared, with a maximum of 1200 ms. The SSD started

126 at 300 ms and was increased and decreased with 50 ms after every successful and failed inhibition
127 trial, respectively, for the left and right-hand side independently. This double staircase procedure
128 thus increased inhibition difficulty – by increasing the amount of time between go and stop stimuli –
129 after successful inhibition and vice versa after failed inhibition, which steers towards generating
130 approximately equal numbers of successful and failed inhibition trials. The SSD was not reset
131 between blocks.
132
133 **Data acquisition**
134 *iEEG recordings*
135 Patients were bilaterally implanted with deep brain electrodes (Medtronic model 3387) in the NAc
136 between 2010 and 2012. Stereotactical placement of the electrodes was performed as previously
137 described by van den Munckhof et al. (2013), which included planning based on T1-weighted
138 magnetic resonance images, online measurement over the electrodes to inform when the gray
139 matter target was reached, and subsequent confirmation with a post-operative CT scan. Each
140 electrode contained four contact points, each being 1.5 mm in length and separated by 0.5 mm. The
141 most ventral contact point was positioned in the NAc core, with the other contact points extending
142 into the ventral part of the anterior limb of the internal capsule. Our sample performed the SST on
143 day four post-surgery for implantation of the deep brain electrodes, except for patient 7, who was
144 tested on the fifth day post-surgery. Patients would later undergo surgery for implantation of the
145 stimulator.
146
147 *EEG recordings*
148 EEG was recorded at a sampling rate of 512 Hz using a 64-channel recording system with shielded
149 Ag/AgCl electrodes (Advanced Neuro Technology B.V.) following the international 10–10 system. Of
150 the 64 channels, eight (four per electrode) were used for the iEEG and four for collecting horizontal

and vertical eye-movement. No signals were recorded from the areas covered by post-surgery bandages. Data were online common average referenced.

**Data analysis**

*Behavioral performance*

Performance measures were calculated over all trials available before artefact rejection. Stop signal reaction time was calculated using the quantile method (Verbruggen and Logan, 2009), which is less susceptible to violations of assumptions underlying the horse-race model than other methods (Band et al., 2003; Verbruggen and Logan, 2009). Per individual, this included calculating the quantile reaction time (QRT), which is the correct go trial reaction time (sorted ascendingly) corresponding to the quantile of the proportion of failed stop trials, and subsequently subtracting the mean SSD.

*Preprocessing*

Data were preprocessed using the EEGLAB-toolbox (version 14.1.1; Delorme and Makeig, 2004) in Matlab (version R2014b; The MathWorks, Inc.). Signals with a standard deviation (SD) below 10% of the median or more than 10 times the median – for EEG and iEEG signals separately – were considered flatlines and too noisy, respectively, and rejected. Then, signals were re-referenced to the average of the respective signal type, i.e. EEG and iEEG. For iEEG, this was done separately for the left and right hemispheres. Signals were band-pass filtered (FIR filter with Hamming window) between 1 and 47 Hz and down-sampled to 256 Hz. The latter was done to improve performance of the EEGLAB-plugin Automatic Artefact Rejection (Gomez-Herrero et al., 2006), using canonical correlation analysis algorithms for blind source separation, which was adopted for automatic removal of muscular artefacts in the EEG signals only. Subsequently, EEG signals were visually inspected and channels considered too noisy were rejected, after which they again were re-referenced to the mean of remaining channels. Then, we extracted epochs from -1000 to 1200 ms relative to go stimulus onset, which we corrected for baseline activity and visually inspected to reject epochs containing

177 artifacts (all except eye blinks). We used principal component analysis to reduce data dimensionality
178 to 45 components (with the exception of 42 components for one patients with less than 45 EEG
179 channels at this point) and exclude minor components. We then ran an independent component
180 analysis on the remaining signals and rejected components containing eye blinks and other noise. We
181 then extracted two subsets of data; from -550 to 550 ms relative to stop signal onset (stop trials only)
182 and to motor response (correct go and failed inhibition trials). For the latter, we excluded trials that
183 contained multiple motor responses and randomly selected an equal number of go trials to keep the
184 number of trials equal between conditions, as there were less failed inhibition than go trials available
185 per participant. We did not do this for the stop trials, because of their limited numbers. Based on
186 previous literature (Cohen et al., 2009; Horschig et al., 2015), we filtered all signals (using a FIR filter
187 with Hamming window) in the theta (4-8 Hz) and alpha (8-13 Hz) frequency ranges. To check for
188 potential relevance of beta oscillations, we looked at overall task beta connectivity. For this, we
189 calculated amplitude envelope correlation (AEC), an amplitude-based connectivity measure that
190 allows for some variability in frequency between signals (further description below), for the theta,
191 alpha, and beta (13-30 Hz) frequency bands between bilateral NAc and 30 randomly selected surface
192 EEG channels on overall task data (per subject an average of 256 trials of all conditions combined,
193 lasting from -500 to 2200 ms relative to the go signal). We then compared these frequency bands
194 using a one-way ANOVA ($F(2,18)=4.12$, $p=.034$) and subsequent two-sample t-tests, which indicated
195 significantly less connectivity in the beta band, compared to the theta ($t(12)=2.7$, $p=.019$) and alpha
196 ($t(12)=2.97$, $p=.012$) bands. Figure 1 depicts AEC on the overall task per frequency band, averaged
197 over the NAc - surface EEG channels pairs, for the left and right NAc separately, as well as the
198 topology of the selected surface electrodes. Based hereon, beta-band oscillations were excluded
199 from further analyses.

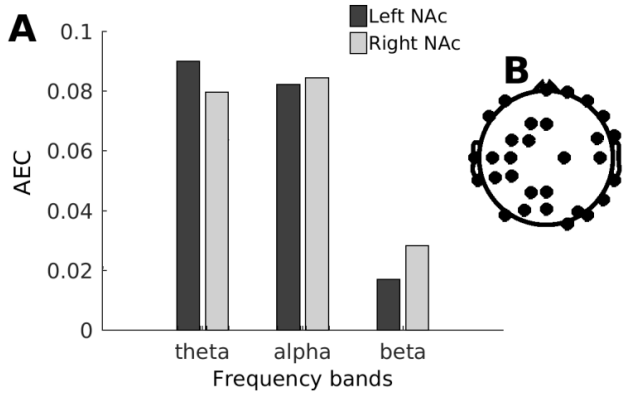


**Figure 1. Amplitude envelope correlation (AEC) in the theta (4-8 Hz), alpha (8-13 Hz), and beta (13-30 Hz) frequency bands on the overall task.** (A) The bars depict average AEC between the NAc (most ventral contact point of the DBS electrode) and 30 randomly selected surface EEG channels, for the left and right NAc separately. (B) topology of the 30 randomly selected surface electrodes

*Connectivity measures*

We have adopted two complementary connectivity measures that rely on different oscillatory characteristics to detect coupling between anatomically distributed sources: amplitude and phase. Firstly, amplitude envelope correlation (AEC) detects coupling based on correlated amplitude modulations - thought to reflect the extent of synchrony of neural assemblies (Varela et al., 2001), thus independently of presence of phase coherence and differences in frequency. This method was found a suitable complementary measure to coherence for detecting longer-range, polysynaptic, cortical gamma interaction in humans (Bruns et al., 2000) and subcortical-cortical beta-gamma coupling in LFPs recorded in cats (Bekisz and Wróbel, 1999). We calculated AEC by correlating the Hilbert envelopes of the signals. Secondly, directed phase transfer entropy (dPTE) estimates the direction of information flow using transfer entropy between instantaneous phase time-series. It was implemented as described in detail by Lobier and colleagues (2014), who showed that it quantifies directed connectivity in a model-free manner that is robust to realistic amounts of noise and linear mixing. First, timeseries were complex filtered using the *Hilbert* transform, then the phase angle was

extracted from the complex signals using *angle*, which were put in a range of 0 – 2*pi. The phases were binned using the number of bins defined in Scott (1992). These binned phases were compared to phases of the second signal after a predefined lag of approximately 10 ms. Since lag precision was restricted by sampling rate, ultimately, approximation of the 10 ms interaction lag was 11.7 ms. Transfer entropy, which is based on the principle that, if signal X influences signal Y, the probability density of signal Y's future conditioned on its past should differ from that conditioned on the pasts both signals X and Y (Schreiber, 2000), with the probability density quantified by Shannon Entropy (Shannon, 1948). Lastly, dPTE was normalized using the marginal probability densities (i.e. within signal transfer entrophies), resulting in values ranging between 0 and 1, with 0.5-1 indicating influence of X over Y, 0-0.5 indicating influence of Y over X, and 0.5 indicating absence of preferential direction of information flow. We used Matlab to implement dPTE. We calculated both connectivity measures over the entire trial lengths to optimize the accuracy of the low frequency phase estimates, considering their strong dependence hereon.

*Power Spectral Density*

We calculated power spectral density (PSD) separately for the 550 ms before and after the event (stop signal onset or motor response). To this end, we first applied a fast Fourier transform. Then, to calculate PSD in decibel (dB), we used this Fourier transformed data as input for the following formula: *10*log10(((1/(srate*sum(slength))) * abs(F).^2)*2)*, where F is the Fourier transformed data, srate is the sampling rate, and slength is the number of samples in the signal. With a frequency resolution of 1.8 Hz, we averaged the PSD at approximately 3.6, 5.4, and 7.2 Hz for the theta frequency PSD and 9, 10.8, and 12.6 Hz for the alpha frequency PSD. From here on out, we will refer to PSD as *power*.

*Statistical analyses*

We employed three levels of correction in this descriptive study. Firstly, to account for the dependency across trials within subject, we applied linear mixed-effects modeling (LMM; Matlab's *fitlme*) with random effects for subject. Secondly, to correct for the total number of channels tested and account for non-normality, we employed 10.000-iteration permutation tests with maximum and minimum t-distributions. This is a method generally used to control the family wise error rate in neuroimaging research, yet it is also suitable for electrophysiological data (Kilner et al., 2005). Thirdly, we Bonferroni-corrected for the number of frequency bands, connectivity measures, and hemispheres tested. We tested the most ventral iEEG channel per hemisphere, located in the NAc, and EEG channels that previously showed connectivity with the NAc during cognitive flexibility (Horschig et al., 2015). These were channels Fp1, Fpz, Fp2, AF7, F7, F1, Fz, FCz, P1, Pz, P2, POz, PO4, O1, and O2. Since subject 6 lacked usable signal from the right NAc, analyses on this channel are based on 6 instead of 7 participants.

For the connectivity analyses, the LMM included random effects for subject and a fixed effect for condition. We tested the connectivity measures separately and over the entire epoch – as opposed to pre. Per iteration of the permutation test, we first randomly shuffled the condition labels within subject before fitting the LMM. The labels were identically shuffled for theta and alpha-filtered signals. Then, we took the maximum and minimum t-values *across all channels* to form the null distributions. For dPTE, the $2{,}5^{th}$ percentile of the minimum t-distribution and the $97.5^{th}$ percentile of the maximum t-distribution constituted the critical values for the lower and upper tails, respectively, consistent with two-tailed testing. Because dPTE is a directed measure, testing both tails reflects testing for both cortex-to-NAc and NAc-to-cortex communication. For AEC, the $95^{th}$ percentile of the maximum t-distribution constituted the critical value for the upper tail, consistent with one-tailed testing. This reflect testing for coupling, but not decoupling, of signals. Ultimately, we Bonferroni-corrected for 4 comparisons (2 frequency bands*2 connectivity measures), resulting in a critical p-value of 0.0125.

For the power analyses, the LMM included random effects for subject and fixed effects for condition, time, and the interaction between condition and time (pre versus post event). We shuffled the condition labels within subject and time-period (pre or post event), formed null distributions of the maximum and minimum t-values per iteration and performed two-tailed tests as described above. Yet, here we tested the iEEG channels against their individual null distributions instead of being collapsed with the EEG channels (and corrected for this via Bonferroni correction), whereas the null distributions for the EEG channels were based on all EEG channels (identical to the connectivity analyses), thereby correcting for the number of channels tested. Ultimately, we Bonferroni-corrected the iEEG channels for 4 comparisons (2 frequency bands*2 hemispheres) and the EEG channels for 2 comparisons (2 frequency bands), resulting in critical p-values of 0.0125 and 0.025, respectively.

*Post-hoc testing*

Significant condition effects in connectivity were subjected to post hoc testing to inform about the timing of the found effect. This included calculating the relevant connectivity measure for a 500-ms sliding window with a stepsize of 23.4 ms, resulting in 26 time windows. For stepsize, we approximated 25 ms, yet precision was restricted by sampling rate. Solely for visualization purposes, we interpolated missing electrodes using spherical spline interpolation (EEGLAB toolbox). For visualization of the sliding window analysis, we oversampled (factor 5) and smoothed (2-point moving average, i.e. 10-point for the oversampled data) the data.

To see whether significant condition effects in connectivity were specific to the most ventrally located contact point of the DBS electrode (L/R0) – targeted at the NAc, we tested whether the effect(s) could also be found on the most dorsally located DBS contact point (L/R3). ). As expected, when average referencing included R0, power spectra for R3 consistently showed lower power than when average referencing excluded R0. This suggests that the signal measured at L/R0 contains considerably higher spectral power. Therefore, we referenced L/R3 against all available other contact points of the DBS electrode (L/R1/ L/R2) except for L/R0. For just comparison, we

repeated the 10.000-iteration permutation test, using the signals from L/R3 instead of L/R0 to calculate connectivity with the surface electrodes. Lastly, considering hemispheric lateralization of motor planning and execution (Sabate et al., 2004), we checked for lateralization of significant connectivity results by adding a main effect of side (left/right trial) and its interaction with condition to the LMM and applying this to the relevant channel pair(s).

For significant power results, we calculated the percentage of change in power over time using the following formula: (10^(diff/10) -1)*100, where diff is the difference in grand average from pre to post event. Additionally, we tested whether alpha and theta power changes were related on a trial-by-trial basis by applying LMMs on the pre-to-post power changes with random effects for subject. We also tested whether significant power modulations were specific to the most ventrally located contact point of the DBS electrode (L/R0) or could also be found on the most dorsally located contact point (L/R3). L/R3 was tested against its own maximum-t distribution, resulting from a 10.000-iteration permutation. Lastly, we checked for lateralization of power modulation by adding a main effect of side (left/right trial) and its interactions with condition and time (pre or post event) to the LMM and applying this to the relevant channel pair(s).

## Results

### Task performance

Table 1 shows sample characteristics and behavioral performance. On average, participants showed an SSRT of 255 ms, indicative of the time required to inhibit an already initiated motor response, they successfully inhibited their response in 52% of stop trials, and either failed to respond or responded incorrectly in 2% of go trials. Mean reaction times on correct go and failed inhibition trials were 679 and 594 ms, respectively. The former seems considerably longer and somewhat more variable than generally reported for both healthy participants and OCD patients (Penades et al., 2007; Boisseau et al., 2012). However, whereas OCD patients usually show longer SSRTs than controls (Lipszyc and Schachar, 2010), current SSRT lies within the ranges reported for both controls and patients;

seemingly somewhere in between their means, yet the literature shows considerable variability. Notably, the depressed participants showed the most omissions (13 and 2%) on go trials.

**Table 1. Subject information and stop signal task performance**

| ID | Sex | Age | Diagnosis | SSRT | mean SSD | mean RT correct go | mean RT failed inhibition | % successful inhibition | % incorrect go |
|---|---|---|---|---|---|---|---|---|---|
| **Patient 1** | F | 40 | OCD | 238 | 653 | 925 | 840 | 58 | 1 |
| **Patient 2** | F | 22 | OCD | 291 | 164 | 473 | 400 | 46 | 0 |
| **Patient 3** | F | 32 | OCD | 305 | 138 | 433 | 412 | 44 | 0 |
| **Patient 4** | F | 31 | OCD | 233 | 587 | 853 | 744 | 60 | 2 |
| **Patient 5** | F | 63 | MDD | 308 | 271 | 625 | 541 | 53 | 13 |
| **Patient 6** | M | 55 | MDD | 179 | 667 | 840 | 732 | 52 | 2 |
| **Patient 7** | M | 37 | SUD | 232 | 354 | 606 | 486 | 53 | 0 |
| **Summary mean (SD)** | 5F/2M | 40 (14.3) | | 255 (47.9) | 405 (228.4) | 679 (194.9) | 594 (176.7) | 52 % (5.6) | 2 % (4.6) |

Abbreviations: SSRT = stop signal reaction time; SSD = stop signal delay; RT = reaction time; SD = standard deviation; F/M = female/male; OCD = obsessive compulsive disorder; MDD = major depressive disorder; SUD = substance use disorder.

**Table 2. Channel availability.**

| ID | Intracranial contact points rejected [a] | EEG channels missing from selection | Number of EEG channels rejected | Number of EEG channels not recorded |
|---|---|---|---|---|
| **Patient 1** | R1 | AF7 | 3, including AF7 | 9 |
| **Patient 2** | R2 | AF7 | 1, including AF7 | 9 |
| **Patient 3** | R1 | O1, Oz, O2 | 6, including O1, Oz, O2 | 8 |
| **Patient 4** | R2 | Fp2 | 6 | 8 |
| **Patient 5** | R1 | | 0 | 6 |
| **Patient 6** | R0, R1 | AF7 | 10, including AF7 | 10 |
| **Patient 7** | | | 4 | 8 |

[a] R = right hemisphere, 0 = most ventral contact point, located in the nucleus accumbens, 1-2 = contact points one and two places, respectively, more dorsal from the most ventral contact point/NAc.

**Connectivity between NAc and the cortex**

When comparing connectivity during the -550 to 550 ms relative to stop signal onset between successful and failed inhibition trials, we found that inhibition success was associated with more negative dPTE between the right NAc and Fpz in the theta-band (figure 2A; table 2). This effect was stable across subjects (figure 2B). Post-hoc sliding window analysis revealed that this effect, which reflects information flow from the NAc to Fpz, was already present before stop stimulus onset (figure

2C). This effect was not different for left versus right trials (t(462)=0.73, p=.466), nor did it show an interaction effect between condition and side (t(462)=0.28, p=.779). Furthermore, theta band dPTE between R3, the most dorsally located DBS contact point, and Fpz did not show a significant condition effect (t(464)=2.52, p=.073, p-Bonferroni-corrected=.291), suggesting that the effect is local to R0, the most ventrally located DBS contact points, targeted at the NAc. No effects were found for AEC or connectivity in the alpha-band.

When comparing connectivity during the -550 to 550 ms relative to motor response between failed inhibition and correct go trials, we did not find any effects after Bonferroni correction. Before correction for 4 comparisons, we saw more positive AEC between the right NAc and O1 in the theta-band (t(464)=2.76, p=.0442) and more positive dPTE between the left NAc and P1 in the alpha-band (t(519)=3.21, p=.022; table 3) on failed inhibition compared to correct go trials.

**Figure 2. Effect of inhibition success on directed phase transfer entropy (dPTE) between right nucleus accumbens (NAc) and scalp electrodes.** (A) dPTE between right NAc and EEG electrode Fpz (large dot) showed a condition effect in the theta-band on successful versus failed inhibition trials (-550 to 550 ms relative to stop stimulus onset). Linear mixed model t-values are plotted with small dots indicating tested channels. (B) Mean dPTE (arbitrary units, centered) for conditions and patients separately. Positive and negative values indicate cortex→NAc and NAc→cortex information flow, respectively. Error bars indicate standard error of the mean. (C) Post-hoc sliding window analysis showed the effect was highest just before stop stimulus onset. Condition effect t-values (solid line) were smoothed and plotted on the left Y-axis, whereas the right Y-axis reflects centered smoothed dPTE intercepts (dashed lines) for the separate conditions, with negative values again indicating effective connectivity from the NAc towards the cortex and vice versa. Since dPTE was calculated for a sliding window, with each dot representing 500 ms, the approximately -290 to 290 ms shown on the X-axis represents the entire -550 to 550 ms trial length.

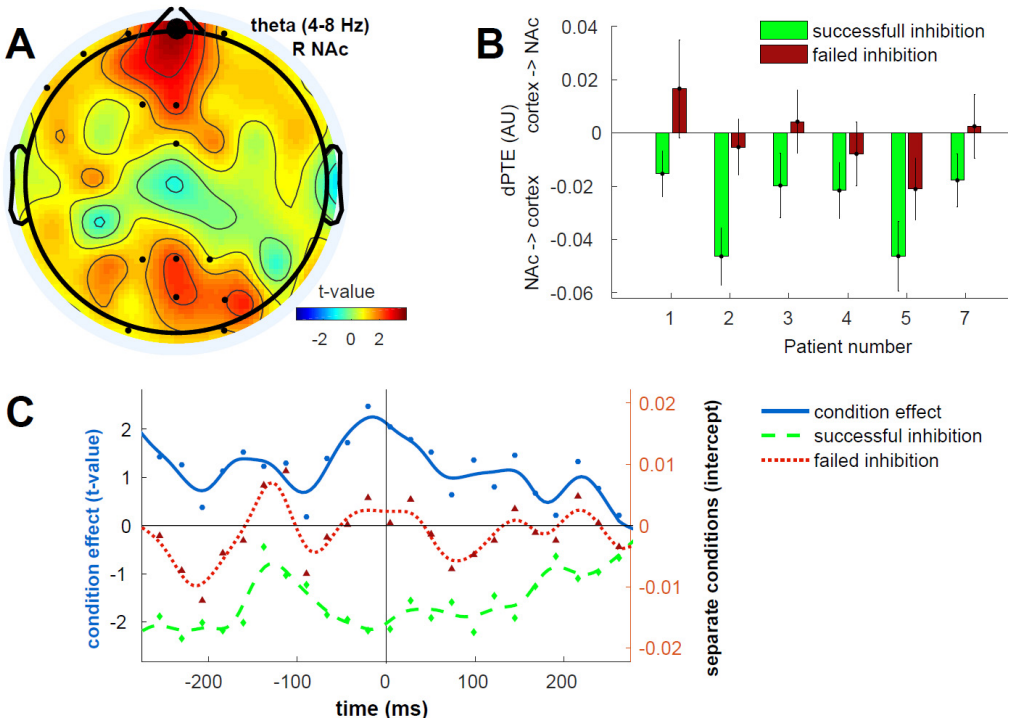


**Table 3. Condition effects in connectivity between NAc and the cortex**

| Time-locking: conditions | Connectivity measure | Frequency band | NAc hemisphere | EEG | t-value | p-value before Bonferroni correction | p-value after Bonferroni correction |
|---|---|---|---|---|---|---|---|
| **Stop: successful vs failed inhibition** | dPTE | theta | R | Fpz | -3.70 | 0.0030 | 0.0120 |
| **Response: failed inhibition vs correct go** * | AEC | theta | R | O1 | 2.76 | 0.0442 | 0.1768 |
| | dPTE | alpha | L | P1 | 3.21 | 0.0220 | 0.0880 |

* Solely significant before Bonferroni correction

**Power modulation in the NAc and the cortex**

When comparing power between successful and failed inhibition trials and changes between the 550 ms pre vs post stop signal onset, we did not find significant effects for condition or the interaction

between time and condition after Bonferroni correction. Neither theta nor alpha power modulation around stop signal onset seems to underlie inhibition success.

When comparing power between failed inhibition and correct go trials and changes between the 550 ms pre vs post motor response, we found a greater theta power increase after response on failed inhibition trials compared to correct go trials in the left NAc and at electrode FCz (figure 2A-B; table 4). This was accompanied by a greater decrease in alpha power at electrode PO4 (figure 2C). These changes in power from pre to post response on correct go and failed inhibition trials, respectively, were 5 and 43% for the left NAc, 10 and 75% for FCz, and 1 and 29% for PO4. Figures 2D-F show the variability of these effects over subjects. We found no lateralization of theta power modulation in the left NAc (side: $t(872)=0.44$, $p=.657$; side*condition*time: $t=1.73$, $p=.083$) or FCz (side: $t=0.11$, $p=.911$; side*condition*time: $t=0.13$, $p=.894$), nor of alpha power modulation on PO4 (side: $t=0.43$, $p=.669$; side*condition*time: $t=0.40$, $p=.689$). Before Bonferroni correction for 4 comparisons, we additionally found an effect of condition on alpha power in the left NAc, showing 13% more alpha power on failed inhibition compared to correct go trials ($t(876)=1.87$, $p=.0284$). Post-hoc LMMs indicated no significant linear relationship between the changes in alpha power at PO4 and theta power in the left NAc ($t(218)=-1.6$, $p=.1138$) or at FCz ($t(218)=-1.47$, $p=.1430$). Specificity analysis showed a significant, yet somewhat smaller, interaction effect on theta power at the most dorsally located contact point of the left DBS electrode ($t=3.26$, $p=.0007$, p-Bonferroni-corrected=.0028). The effect showed a similar pattern to that found on the most ventrally located contact point, with pre to post response power changes of -1 and 41% on correct go and failed inhibition trials, respectively.

**Figure 3. Power spectral density modulation following response on failed inhibition versus correct go trials.** Power is expressed in decibel (dB). Error bars indicate standard error of the mean. Greater theta power increase following motor response on failed inhibition compared to correct go trials (A) in the left nucleus accumbens and (B) on electrode FCz. (C) Greater alpha power decrease following motor response on failed inhibition compared to correct go trials on electrode PO4. (D-F) Power modulation from plots A-C, respectively, visualized for patients separately. *CG* and *FI* refer to correct go and failed inhibition conditions, respectively.

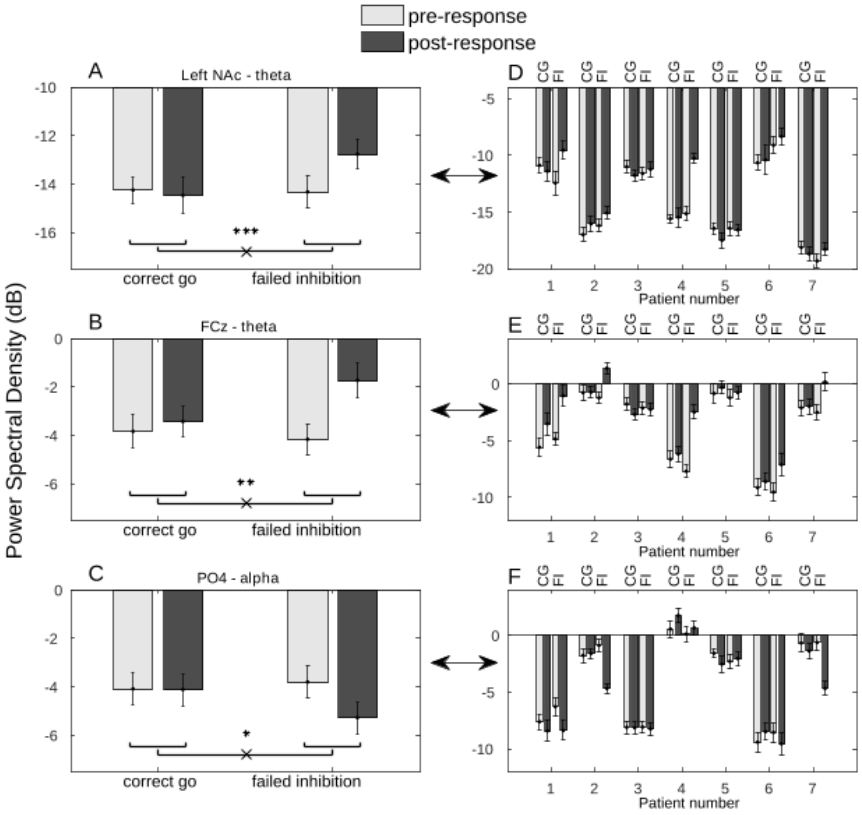

**Table 4. Power spectral density modulation following motor response on failed inhibition versus correct go trials**

| Frequency band | Effect | Channel | t-value | p-value before Bonferroni correction | p-value after Bonferroni correction |
|---|---|---|---|---|---|
| theta | condition*time | NAc L | 3.29 | 0.0004 | 0.0016 |
| | condition*time | FCz | 3.94 | 0.0006 | 0.0012 |
| alpha | condition | NAc L | 1.87 | 0.0284 | 0.1136* |
| | condition*time | PO4 | -3.11 | 0.0110 | 0.0220 |

* Solely significant before Bonferroni correction

## Discussion

We found that inhibition success – as opposed to failure – was associated with increased information flow from right NAc to medial frontal cortex through phase coupling of theta oscillations, present already before stop signal onset. We additionally found that theta power increased following motor response on failed inhibition compared to correct go trials in both the left NAc and medial frontal cortex, whereas parieto-occipital cortex showed an alpha power decrease.

To our knowledge, this is the first report to show involvement of the NAc and its communication with frontal cortex in adaptive behavior pertaining motor control. Lack of significant findings for AEC or in the alpha-band suggests theta phase-specificity of NAc-frontal cortex communication underlying inhibition success. Yet, some trends suggested the possibility of theta amplitude coupling between right NAc and (left) occipital cortex and/or alpha phase coupling between the left NAc and (left) parietal cortex to distinguish between correct going and failed inhibition.

The observed connectivity is consistent with the finding of NAc-to-frontal cortex theta-band granger causality during anticipation of a visual stimulus during a task of cognitive flexibility (Horschig et al., 2015). We likewise found that communication was already present before – and sustained

around – stimulus presentation. Computational models suggest that the ventral striatum might actively gate sensory information based on task demands maintained in frontal regions of cognitive control (Frank et al., 2001). This idea was previously substantiated by showing that the NAc modulated fronto-parietal coherence in the alpha-band, which is in line with a nonlinear dynamic causal modeling fMRI study showing that shifts in attention relied on the ventral striatopallidum to modulate connectivity between stimulus-specific visual association areas and the prefrontal cortex (van Schouwenburg et al., 2010). Therefore, the currently found pre-stimulus phase coupling between NAc and frontal cortex might likewise reflect facilitation of task-relevant information. Considering the visual SST, this information likely originates from visual cortex and flows via the globus pallidus, subthalamic nucleus, and thalamus to frontal cortex (Haber et al., 1995; Haber and Knutson, 2010). In line with this view, we found a trend towards theta amplitude coupling between right NAc and electrode O1. These findings extend the well-established role of the NAc in reward processing and reinforcement learning (Cohen et al., 2008; Lega et al., 2011; Cohen et al., 2012; Patel et al., 2012) to the context of adaptive behavior in tasks of both cognitive and behavioral flexibility.

Yet, we did not observe the post-stimulus increase in information flow from the NAc to the cortex that was previously found (Horschig et al., 2015). This might be explained by task differences, since stimulus presentation in the former task required redirection of attention and a subsequent button press, whereas it required inhibition of a button press in the present task. In addition, it previously was unclear whether the effects relied on phase or amplitude locking, because granger causality depends on both such signal components (Lobier et al., 2014). We now extend those findings by showing that the information flow from the NAc to the cortex depends on theta phase synchronization, rather than amplitude coupling. In contrast to other intracranial studies that found connectivity from the cortex to the NAc during attentional switching and reward anticipation, we did not find information flow from the cortex to the NAc, being indicative of cognitive control, to underlie inhibition success (Cohen et al., 2012; Horschig et al., 2015).

We additionally found an increase in midfrontal and left NAc theta power as well as a decrease in parieto-occipital alpha power after response on failed inhibition compared to correct go trials. Theta power increases in both NAc and medial frontal cortex have previously been found following – especially negative – feedback on a variety of tasks (Cohen et al., 2007; Münte et al., 2008; Cohen et al., 2009; Nurislamova et al., 2019). The well-established feedback or error-related negativity, evoked by erroneous (motor) responses, has been found to arise from a combination of a power increase and partial phase synchronization of theta oscillations (Luu et al., 2004; Trujillo and Allen, 2007). These signals have been traced back to the anterior cingulate cortex and/or pre-SMA, which are involved in error- and conflict processing and subsequent behavioral adjustment (Garavan et al., 2002; Luu et al., 2004; Iannaccone et al., 2015). Interestingly, it has been postulated that, whereas high theta might reflect the conflict monitoring process itself, low theta underlies the more general process of interregional communication and thus relays the error to other areas of cognitive control (Huster et al., 2013). Current power increases were more pronounced for lower theta frequencies – especially so for electrode FCz, pointing to engagement of cognitive control after failed inhibition. Performance monitoring-related theta power increases often co-occur with increased theta phase-synchronization between medial frontal and parietal cortex (Nurislamova et al., 2019), which was previously found to be modulated by the NAc during attentional switching (Horschig et al., 2015). Although we found a concurrent decrease in posterior alpha power – something previously found to accompany midfrontal theta increases following failed inhibition on a Go/NoGo task (Mazaheri et al., 2009) – these theta and alpha power modulations were not significantly related on a trial-by-trial basis. Yet, with p=.11 and p=.14 for those relationships, this might have resulted from our limited sample size. Alpha power increases are thought to decrease local neural processing capacity, thereby inhibiting a region's activity (Jensen and Mazaheri, 2010). Therefore, our alpha power decrease might reflect release of inhibition on the posterior parietal regions involved in action planning and decision making, likely resulting from top–down influence of the frontal control system (Andersen and Cui, 2009).

In conclusion, our results supplement current knowledge about cortical involvement in performance monitoring by implicating NAc theta power modulation in the engagement of cognitive control after inhibition failure, possibly for subsequent adjustment of decision-making parameters to prevent additional errors. This extends the previous finding that subthalamic nucleus theta power and coherence with frontal cortex are likewise modulated during the SST (Alegre et al., 2013). Similar to the theta power increases we found in the NAc and frontal cortex and relate to the well-established error-related negativity, the subthalamic nucleus showed inhibition failure-related increases in theta power and coherence with frontal cortex. If and how communications between these subcortical structures underlies feedback processing remains unanswered, yet these findings point to a role of theta oscillations herein. Additionally, we found inhibition success-related theta connectivity between the NAc and frontal cortex that was absent in the subthalamic nucleus. Although the inhibition success-related connectivity was specific to the most ventrally located contact point of the right DBS electrode – targeted at the NAc, we found the post-response theta power increase also on the most dorsally located contact point of the left DBS electrode. Although all targeted at the NAc, slight differences in DBS electrode location between patients could explain this non-specificity, considering that the medially located contact points were used as reference. Alternatively, it could be that the power change is not restricted to the grey matter of the NAc. Lack of significant lateralization of our main effects substantiates their interpretation as higher-order regulatory rather than primary motor processes (Sabate et al., 2004).

Notwithstanding the unique dataset, it comes with some limitations. First of all, although we allowed for random effects for subject in our models, the sample size of seven subjects limits statistical power and generalizability of the results. To account for this and limit (unnecessary) multiple comparison correction, we tested a selection of EEG channels based on previous research (Horschig et al., 2015), yet thereby limiting exploration of potentially unexpected findings. Also, we were unable to measure the impedances of the DBS electrode contact points – informative of signal quality, since doing so could potentially induce non-therapeutic stimulation. Furthermore, we must

keep in mind that our results might represent pathological brain functioning, since we used a severely affected psychiatric sample and lacked a control group. Especially so since NAc-DBS is thought to exert its therapeutic effects through targeting NA-cortical connectivity (Figee et al., 2013; Smolders et al., 2013). Also, MDD patients show aberrant error-related negativity (Tucker et al., 2003; Holmes and Pizzagalli, 2008), which has been linked to midline frontal theta oscillations during action regulation (Luu and Tucker, 2001). However, cortical feedback-related negativity has been found not to differ between controls and DBS-implanted OCD and Tourette's Syndrome patients (Schuller et al., 2015) and we found stable and significant results in a sample that included various disorders, albeit mainly disorders of compulsivity. Moreover, participants were not taking SSRIs at the time of data collection, yet post-surgical analgesics could have affected brain functioning.

We found condition-specific phase-synchronization and power modulation for separate time periods of task performance, yet associations between oscillatory phase and power, a phenomenon called cross-frequency coupling, have additionally been reported. Coupling of gamma power to alpha phase in the NAc was found during reward processing (Cohen et al., 2008), decreased before strategic switching (Cohen et al., 2009), and differentiated between positive and negative feedback (Lega et al., 2011). Moreover, NAc gamma-theta coupling varied with cognitive control during a motor learning task (Dürschmid, 2013). To gain more insight into the interplay between subcortical and cortical local cross-frequency coupling and phase synchronization between distant regions, such associations should be tested directly using datasets such as ours. Additionally, since increased theta phase-synchronization between bilateral NAc has been linked to behavioral adjustment following losses (Cohen et al., 2009), inter-NAc connectivity might also be relevant for SST performance. Lastly, the possibility of functional hemispheric differentiation of the NAc warrant further investigation, considering we found right lateralized inhibition success-related connectivity changes and left lateralized performance monitoring-related power changes.

## Conclusions

In sum, due to our unique dataset of concurrent striatal and EEG recordings, we were able to show involvement of pre-stimulus NAc-to-medial frontal cortex theta phase synchronization in successful response inhibition and both cortical and NAc power modulation in the theta and alpha-bands in performance monitoring on the stop signal task. These results corroborate earlier findings that theta oscillations are crucial for cortical-subcortical communication during cognitive processing and involvement of the NAc in adaptive behavior. Yet, still plenty remains to be learned about both the specificity and the extent of interplay of different features of oscillatory activity, including cross-frequency coupling and the relationship between NAc-cortical communication and cortical interactions.

## References

Alegre M, Lopez-Azcarate J, Obeso I, Wilkinson L, Rodriguez-Oroz MC, Valencia M, Garcia-Garcia D, Guridi J, Artieda J, Jahanshahi M, Obeso JA (2013) The subthalamic nucleus is involved in successful inhibition in the stop-signal task: a local field potential study in Parkinson's disease. *Exp Neurol* 239:1-12.

Alexander GE, DeLong MR, Strick PL (1986) Parallel organization of functionally segregated circuits linking basal ganglia and cortex. *Annu Rev Neurosci* 9:357-381.

Andersen RA, Cui H (2009) Intention, action planning, and decision making in parietal-frontal circuits. *Neuron* 63:568-583.

Band GPH, van der Model MW, Logan GD (2003) Horse-race model simulations of the stop-signal procedure. *Acta Psychol (Amst)* 112:105-142.

Bekisz M, Wróbel A (1999) Coupling of beta and gamma activity in cortico-thalamic systems of cats attending to visual stimuli. *Neuroreport* 10:3589-3594.

Bissett PG, Logan GD (2011) Balancing cognitive demands: control adjustments in the stop-signal paradigm. *J Exp Psychol Learn Mem Cogn* 37:392-404.

560 Boisseau CL, Thompson-Brenner H, Caldwell-Harris C, Pratt E, Farchione T, Barlow DH (2012)
561 Behavioral and cognitive impulsivity in obsessive-compulsive disorder and eating disorders.
562 *Psychiatry Res* 200:1062-1066.
563 Bruns A, Eckhorn R, Jokeit H, Ebner A (2000) Amplitude Envelope Correlation detects coupling among
564 incoherent brain signals. *Neuroreport* 11:1509-1514.
565 Cohen MX, Axmacher N, Lenartz D, Elger CE, Sturm V, Schlaepfer TE (2008) Good Vibrations: Cross-
566 frequency Coupling in the Human Nucleus Accumbens during Reward Processing. *J Cogn Neurosci*
567 21:875-889.
568 Cohen MX, Axmacher N, Lenartz D, Elger CE, Sturm V, Schlaepfer TE (2009) Nuclei accumbens phase
569 synchrony predicts decision-making reversals following negative feedback. *J Neurosci* 29:7591-7598.
570 Cohen MX, Bour L, Mantione M, Figee M, Vink M, Tijssen MA, van Rootselaar AF, van den Munckhof
571 P, Schuurman PR, Denys D (2012) Top-down-directed synchrony from medial frontal cortex to
572 nucleus accumbens during reward anticipation. *Hum Brain Mapp* 33:246-252.
573 Cohen MX, Elger CE, Ranganath C (2007) Reward expectation modulates feedback-related negativity
574 and EEG spectra. *Neuroimage* 35:968-978.
575 Delorme A, Makeig S (2004) EEGLAB: an open source toolbox for analysis of single-trial EEG dynamics
576 including independent component analysis. *J Neurosci Methods* 134:9-21.
577 Dürschmid S (2013) Phase-amplitude cross-frequency coupling in the human nucleus accumbens
578 tracks action monitoring during cognitive control. *Front Hum Neurosci* 7:1-17.
579 Figee M, Luigjes J, Smolders R, Valencia-Alfonso CE, van Wingen G, de Kwaasteniet B, Mantione M,
580 Ooms P, de Koning P, Vulink N, Levar N, Droge L, van den Munckhof P, Schuurman PR, Nederveen A,
581 van den Brink W, Mazaheri A, Vink M, Denys D (2013) Deep brain stimulation restores frontostriatal
582 network activity in obsessive-compulsive disorder. *Nat Neurosci* 16:386-387.
583 Floresco SB, Ghods-Sharifi S, Vexelman C, Magyar O (2006) Dissociable roles for the nucleus
584 accumbens core and shell in regulating set shifting. *J Neurosci* 26:2449-2457.

585 Frank MJ, Loughry B, C. ORR (2001) Interactions between frontal cortex and basal ganglia in working
586 memory: A computational model. *Cognitive, Affective, & Behavioral Neuroscience* 1:137-160.
587 Garavan H, Ross TJ, Murphy K, Roche RA, Stein EA (2002) Dissociable executive functions in the
588 dynamic control of behavior: inhibition, error detection, and correction. *Neuroimage* 17:1820-1829.
589 Gomez-Herrero G, Clercq W, Anwar H, Kara O, Egiazarian K, Huffel S, Paesschen W (2006). Automatic
590 Removal of Ocular Artifacts in the EEG without an EOG Reference Channel. In Proceedings of the 7th
591 Nordic Signal Processing Symposium - NORSIG 2006, pp. 130-133.
592 Haber SN, Knutson B (2010) The reward circuit: linking primate anatomy and human imaging.
593 *Neuropsychopharmacology* 35:4-26.
594 Haber SN, Kunishio K, Mizobuchi M, Lynd-Balta E (1995) The Orbital and Medial Prefrontal Circuit
595 Through the Primate Basal Ganglia. *J Neurosci* 15:4851-4867.
596 Holmes AJ, Pizzagalli DA (2008) Spatiotemporal Dynamics of Error Processing Dysfunctions in Major
597 Depressive Disorder. *Arch Gen Psychiatry* 65:179-188.
598 Horschig JM, Smolders R, Bonnefond M, Schoffelen JM, van den Munckhof P, Schuurman PR, Cools R,
599 Denys D, Jensen O (2015) Directed Communication between Nucleus Accumbens and Neocortex in
600 Humans Is Differentially Supported by Synchronization in the Theta and Alpha Band. *PLoS One*
601 10:e0138685.
602 Huster RJ, Enriquez-Geppert S, Lavallee CF, Falkenstein M, Herrmann CS (2013)
603 Electroencephalography of response inhibition tasks: functional networks and cognitive
604 contributions. *Int J Psychophysiol* 87:217-233.
605 Iannaccone R, Hauser TU, Staempfli P, Walitza S, Brandeis D, Brem S (2015) Conflict monitoring and
606 error processing: new insights from simultaneous EEG-fMRI. *Neuroimage* 105:395-407.
607 Jensen O, Mazaheri A (2010) Shaping functional architecture by oscillatory alpha activity: gating by
608 inhibition. *Front Hum Neurosci* 4:186.
609 Kilner JM, Kiebel SJ, Friston KJ (2005) Applications of random field theory to electrophysiology.
610 *Neurosci Lett* 374:174-178.

611 Lega BC, Kahana MJ, Jaggi J, Baltuch GH, Zaghloul K (2011) Neuronal and oscillatory activity during
612 reward processing in the human ventral striatum. *Neuroreport* 22:795–800.
613 Lipszyc J, Schachar R (2010) Inhibitory control and psychopathology: a meta-analysis of studies using
614 the stop signal task. *J Int Neuropsychol Soc* 16:1064-1076.
615 Lobier M, Siebenhühner F, Palva S, Palva JM (2014) Phase transfer entropy: A novel phase-based
616 measure for directed connectivity in networks coupled by oscillatory interactions. *Neuroimage*
617 85:853-872.
618 Logan GD, Cowan WB (1984) On the Ability to Inhibit Thought and Action: A Theory of an Act of
619 Control. *Psychol Rev* 91:295-327.
620 Luu P, Tucker DM (2001) Regulating action: alternating activiation of midline frontal and motor
621 cortical networks. *Clin Neurophysiol* 112:1295-1306.
622 Luu P, Tucker DM, Makeig S (2004) Frontal midline theta and the error-related negativity:
623 neurophysiological mechanisms of action regulation. *Clin Neurophysiol* 115:1821-1835.
624 Miller EK, Cohen JD (2001) An integrative theory of prefrontal cortex function. *Annu Rev Neurosci*
625 24:167-202.
626 Mogenson GJ, Jones DL, Yim CY (1980) From motivation to action: functional interface between the
627 limbic system and the motor system. *Prog Neurobiol* 14:69-97.
628 Münte TF, Heldmann M, Hinrichs H, J. M-P, Krämer UM, Sturm V, Heinze HJ (2008) Contribution of
629 subcortical structures to cognition assessed with invasive electrophysiology in humans. *Front*
630 *Neurosci* 2:72-78.
631 Nurislamova YM, Novikov NA, Zhozhikashvili NA, Chernyshev BV (2019) Enhanced Theta-Band
632 Coherence Between Midfrontal and Posterior Parietal Areas Reflects Post-feedback Adjustments in
633 the State of Outcome Uncertainty. *Front Integr Neurosci* 13:14.
634 Patel SR, Sheth SA, Mian MK, Gale JT, Greenberg BD, Dougherty DD, Eskandar EN (2012) Single-
635 neuron responses in the human nucleus accumbens during a financial decision-making task. *J*
636 *Neurosci* 32:7311-7315.

637 Penades R, Catalan R, Rubia K, Andres S, Salamero M, Gasto C (2007) Impaired response inhibition in
638 obsessive compulsive disorder. *Eur Psychiatry* 22:404-410.
639 Ray NJ, Brittain JS, Holland P, Joundi RA, Stein JF, Aziz TZ, Jenkinson N (2012) The role of the
640 subthalamic nucleus in response inhibition: evidence from local field potential recordings in the
641 human subthalamic nucleus. *Neuroimage* 60:271-278.
642 Sabate M, Gonzalez B, Rodriguez M (2004) Brain lateralization of motor imagery: motor planning
643 asymmetry as a cause of movement lateralization. *Neuropsychologia* 42:1041-1049.
644 Schreiber T (2000) Measuring Information Transfer. *Phys Rev Lett* 85:461-464.
645 Schuller T, Gruendler TO, Jocham G, Klein TA, Timmermann L, Visser-Vandewalle V, Kuhn J, Ullsperger
646 M (2015) Rapid feedback processing in human nucleus accumbens and motor thalamus.
647 *Neuropsychologia* 70:246-254.
648 Scott DW (1992). Multivariate Density Estimation (New York: Wiley and Sons, Inc.).
649 Shannon CE (1948) A Mathematical Theory of Communication. *The Bell System Technical Journal*
650 27:379-323.
651 Smolders R, Mazaheri A, van Wingen G, Figee M, de Koning PP, Denys D (2013) Deep brain
652 stimulation targeted at the nucleus accumbens decreases the potential for pathologic network
653 communication. *Biol Psychiatry* 74:e27-28.
654 Trujillo LT, Allen JJ (2007) Theta EEG dynamics of the error-related negativity. *Clin Neurophysiol*
655 118:645-668.
656 Tucker DM, Luu P, Frishkoff G, Quiring J, Poulsen C (2003) Frontolimbic response to negative
657 feedback in clinical depression. *J Abnorm Psychol* 112:667-678.
658 van den Munckhof P, Bosch DA, Mantione MH, Figee M, Denys DA, Schuurman PR (2013) Active
659 stimulation site of nucleus accumbens deep brain stimulation in obsessive-compulsive disorder is
660 localized in the ventral internal capsule. *Acta Neurochir Suppl* 117:53-59.
661 van Schouwenburg MR, den Ouden HE, Cools R (2010) The human basal ganglia modulate frontal-
662 posterior connectivity during attention shifting. *J Neurosci* 30:9910-9918.

Varela F, Lachaux J, Rodriguez E, Martinerie J (2001) The brainweb: Phase synchronization and large-scale integration. *Nature Reviews Neuroscience* 2:229-239.

Verbruggen F, Logan GD (2009) Models of response inhibition in the stop-signal and stop-change paradigms. *Neurosci Biobehav Rev* 33:647-661.

Yawata S, Yamaguchi T, Danjo T, Hikida T, Nakanishi S (2012) Pathway-specific control of reward learning and its flexibility via selective dopamine receptors in the nucleus accumbens. *Proc Natl Acad Sci U S A* 109:12764-12769.

## Figure and table legends

**Table 1. Subject information and stop signal task performance**

Abbreviations: SSRT = stop signal reaction time; SSD = stop signal delay; RT = reaction time; SD = standard deviation; F/M = female/male; OCD = obsessive compulsive disorder; MDD = major depressive disorder; SUD = substance use disorder.

**Table 2. Channel availability.**

[a] R = right hemisphere, 0 = most ventral contact point, located in the nucleus accumbens, 1-2 = contact points one and two places, respectively, more dorsal from the most ventral contact point/NAc.

**Figure 1. Amplitude envelope correlation (AEC) in the theta (4-8 Hz), alpha (8-13 Hz), and beta (13-30 Hz) frequency bands on the overall task.** (A) The bars depict average AEC between the NAc (most ventral contact point of the DBS electrode) and 30 randomly selected surface EEG channels, for the left and right NAc separately. (B) topology of the 30 randomly selected surface electrodes.

**Figure 2. Effect of inhibition success on directed phase transfer entropy (dPTE) between right nucleus accumbens (NAc) and scalp electrodes.** (A) dPTE between right NAc and EEG electrode Fpz (large dot) showed a condition effect in the theta-band on successful versus failed inhibition trials (-

550 to 550 ms relative to stop stimulus onset). Linear mixed model t-values are plotted with small dots indicating tested channels. (B) Mean dPTE (arbitrary units, centered) for conditions and patients separately. Positive and negative values indicate cortex→NAc and NAc→cortex information flow, respectively. Error bars indicate standard error of the mean. (C) Post-hoc sliding window analysis showed the effect was highest just before stop stimulus onset. Condition effect t-values (solid line) were smoothed and plotted on the left Y-axis, whereas the right Y-axis reflects centered smoothed dPTE intercepts (dashed lines) for the separate conditions, with negative values again indicating effective connectivity from the NAc towards the cortex and vice versa. Since dPTE was calculated for a sliding window, with each dot representing 500 ms, the approximately -290 to 290 ms shown on the X-axis represents the entire -550 to 550 ms trial length.

**Table 3. Condition effects in connectivity between NAc and the cortex**

* Solely significant before Bonferroni correction

**Figure 3. Power spectral density modulation following response on failed inhibition versus correct go trials.** Power is expressed in decibel (dB). Error bars indicate standard error of the mean. Greater theta power increase following motor response on failed inhibition compared to correct go trials (A) in the left nucleus accumbens and (B) on electrode FCz. (C) Greater alpha power decrease following motor response on failed inhibition compared to correct go trials on electrode PO4. (D-F) Power modulation from plots A-C, respectively, visualized for patients separately. *CG* and *FI* refer to correct go and failed inhibition conditions, respectively.

**Table 4. Power spectral density modulation following motor response on failed inhibition versus correct go trials**

* Solely significant before Bonferroni correction

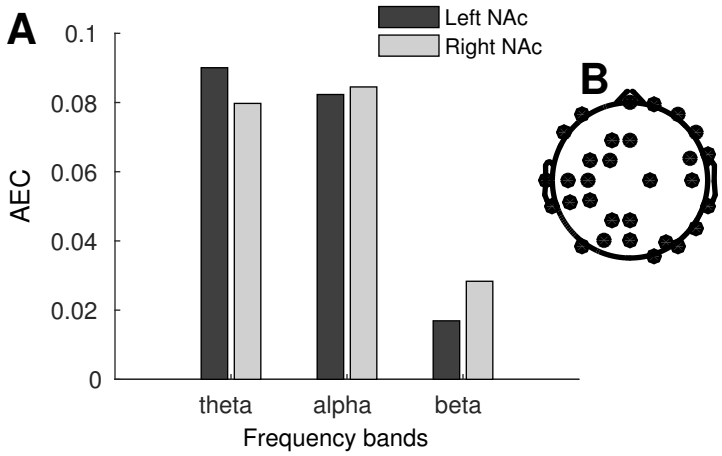

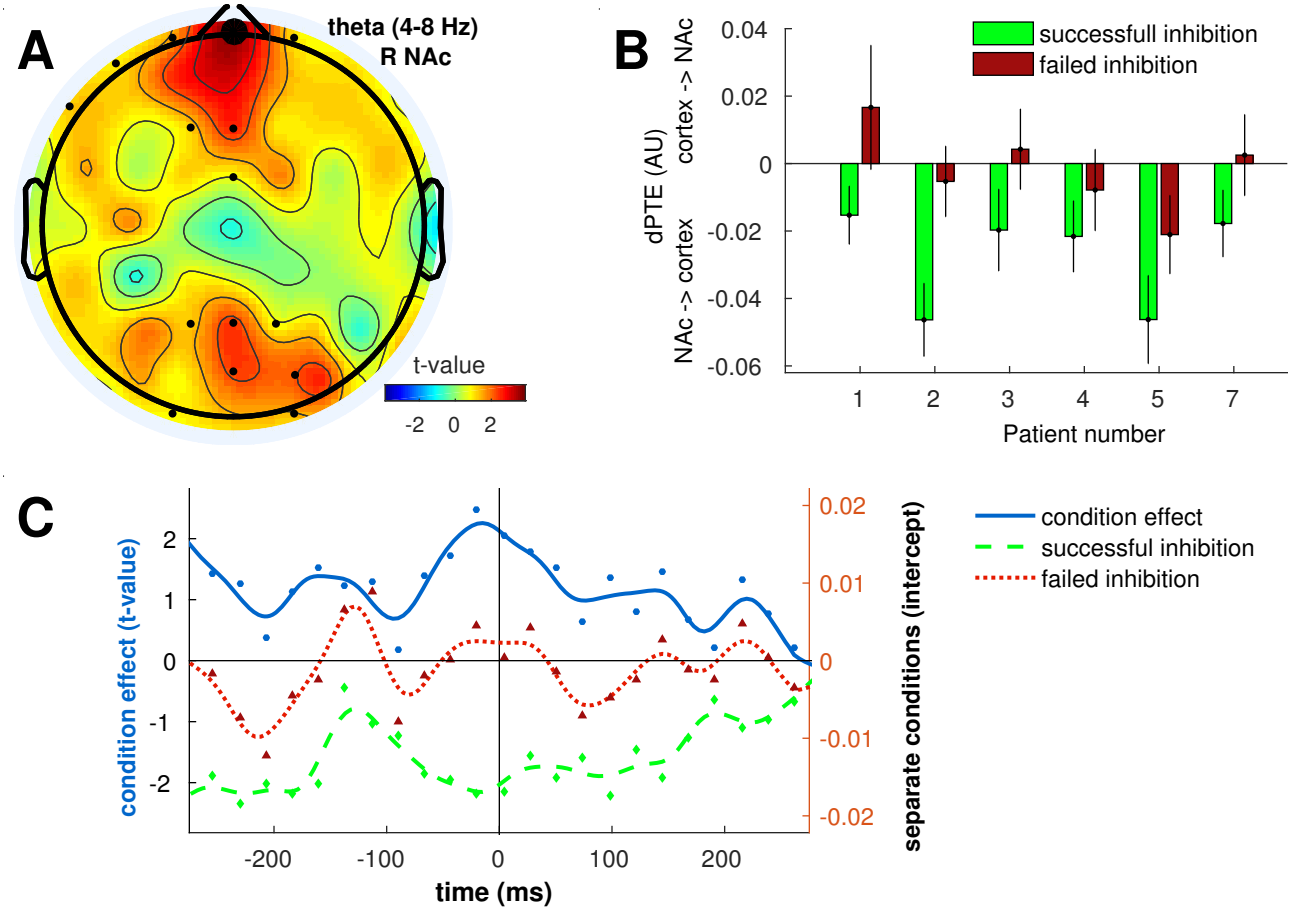

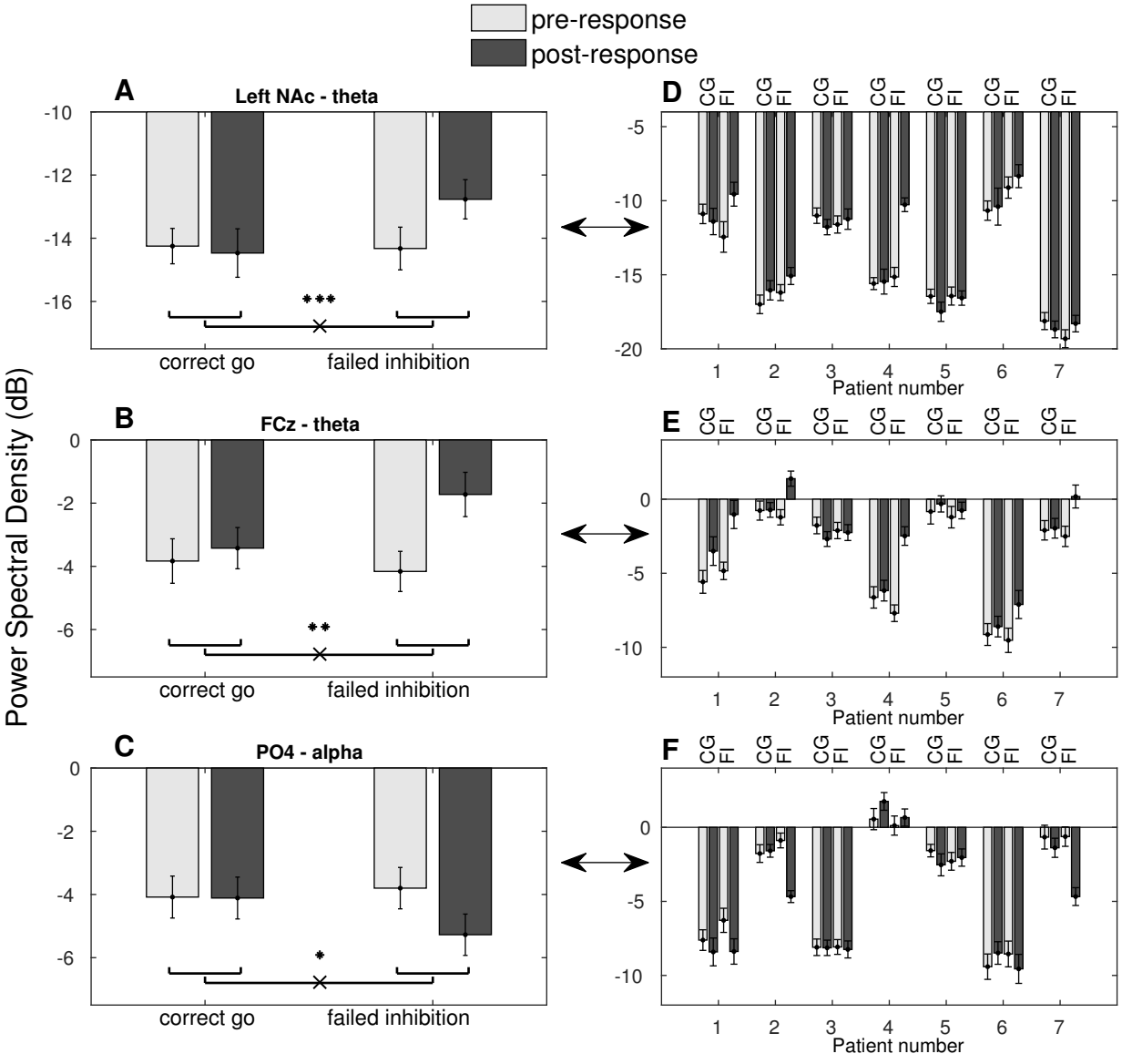

**Table 1. Subject information and stop signal task performance**

| ID | Sex | Age | Diagnosis | SSRT | mean SSD | mean RT correct go | mean RT failed inhibition | % successful inhibition | % incorrect go |
|---|---|---|---|---|---|---|---|---|---|
| **Patient 1** | F | 40 | OCD | 238 | 653 | 925 | 840 | 58 | 1 |
| **Patient 2** | F | 22 | OCD | 291 | 164 | 473 | 400 | 46 | 0 |
| **Patient 3** | F | 32 | OCD | 305 | 138 | 433 | 412 | 44 | 0 |
| **Patient 4** | F | 31 | OCD | 233 | 587 | 853 | 744 | 60 | 2 |
| **Patient 5** | F | 63 | MDD | 308 | 271 | 625 | 541 | 53 | 13 |
| **Patient 6** | M | 55 | MDD | 179 | 667 | 840 | 732 | 52 | 2 |
| **Patient 7** | M | 37 | SUD | 232 | 354 | 606 | 486 | 53 | 0 |
| **Summary** | 5F/2M | 40 | | 255 | 405 | 679 | 594 | 52 % | 2 % |
| **mean (SD)** | | (14.3) | | (47.9) | (228.4) | (194.9) | (176.7) | (5.6) | (4.6) |

Abbreviations: SSRT = stop signal reaction time; SSD = stop signal delay; RT = reaction time; SD = standard deviation; F/M = female/male; OCD = obsessive compulsive disorder; MDD = major depressive disorder; SUD = substance use disorder.

**Table 2. Channel availability.**

| ID | Intracranial contact points rejected [a] | EEG channels missing from selection | Number of EEG channels rejected | Number of EEG channels not recorded |
|---|---|---|---|---|
| **Patient 1** | R1 | AF7 | 3, including AF7 | 9 |
| **Patient 2** | R2 | AF7 | 1, including AF7 | 9 |
| **Patient 3** | R1 | O1, Oz, O2 | 6, including O1, Oz, O2 | 8 |
| **Patient 4** | R2 | Fp2 | 6 | 8 |
| **Patient 5** | R1 | | 0 | 6 |
| **Patient 6** | R0, R1 | AF7 | 10, including AF7 | 10 |
| **Patient 7** | | | 4 | 8 |

[a] R = right hemisphere, 0 = most ventral contact point, located in the nucleus accumbens, 1-2 = contact points one and two places, respectively, more dorsal from the most ventral contact point/NAc.

**Table 3. Condition effects in connectivity between NAc and the cortex**

| Time-locking: conditions | Connectivity measure | Frequency band | NAc hemisphere | EEG | t-value | p-value before Bonferroni correction | p-value after Bonferroni correction |
|---|---|---|---|---|---|---|---|
| **Stop: successful vs failed inhibition** | dPTE | theta | R | Fpz | -3.70 | 0.0030 | 0.0120 |
| **Response:** * **failed inhibition vs correct go** | AEC | theta | R | O1 | 2.76 | 0.0442 | 0.1768 |
| | dPTE | alpha | L | P1 | 3.21 | 0.0220 | 0.0880 |

* Solely significant before Bonferroni correction

**Table 4. Power spectral density modulation following motor response on failed inhibition versus correct go trials**

| Frequency band | Effect | Channel | t-value | p-value before Bonferroni correction | p-value after Bonferroni correction |
|---|---|---|---|---|---|
| theta | condition*time | NAc L | 3.29 | 0.0004 | 0.0016 |
| | condition*time | FCz | 3.94 | 0.0006 | 0.0012 |
| alpha | condition | NAc L | 1.87 | 0.0284 | 0.1136* |
| | condition*time | PO4 | -3.11 | 0.0110 | 0.0220 |

* Solely significant before Bonferroni correction